Plenoptic Sensor : Application to Extend Field-of-View

Benoît Vandame Valter Drazic Matthieu Hog Neus Sabater
Technicolor R & I
975 Avenue des Champs Blancs, 35576 Cesson-Sévigné, France
[benoit.vandame, valter.drazic, matthieu.hog, neus.sabater]@technicolor.com

***Abstract*—In this paper we study the light field sampling produced by ideal plenoptic sensors, an emerging technology providing new optical capabilities. In particular, we leverage its potential with a new optical design that couples a pyramid lens with an ideal plenoptic sensor. The main advantage is that it extends the field-of-view (FOV) of a main-lens without changing its focal length. To evince the utility of the proposed design we have performed different experiments. First, we demonstrate on simulated synthetic images that our optical design effectively doubles the FOV. Then, we show its feasibility with two different prototypes using plenoptic cameras on the market with very different plenoptic samplings, namely a Raytrix R5 and a Canon 5D MarkIV. Arguably, future cameras with ideal plenoptic sensors will be able to be coupled with pyramid lenses to extend its inherent FOV in a single snapshot.**

I. Introduction

Plenoptic cameras are able to capture the Light-Field (LF), thanks to a micro-lens array (MLA) placed between the main-lens and the sensor. Depending on the MLA position, plenoptic cameras are divided in type-1 [1] (e.g. Lytro [2]) and type-2 or focused [3] (e.g. Raytrix [4]).

The first plenoptic cameras on the market have the particularity that the MLA is not well aligned with the sensor. Indeed, plenoptic camera manufacturers assemble individual optic components producing an unavoidable rotation offset between the MLA and the pixel matrix. For this reason, many research works in the field have focused on calibration and decoding methods [5], [6], as well as image processing algorithms taking into account such misalignments [7], [8], [9]. However, camera manufacturers rely on wafer-level fabrication to assemble micro-optical components like MLA's onto pixel matrix with great accuracy. Such *ideal plenoptic sensors* (simply called *plenoptic sensors* in the sequel) provide a new paradigm for LF processing since no camera calibration is required and sub-aperture images (SAI's) or Epipolar Plan Images (EPI's) are simply extracted without interpolation.

In fact, very simple plenoptic sensors already exist in the consumer market. This is the case of dual-pixels (comparable to left and right views of stereo camera) in high-end smartphones such as the Samsung S7 [10], and DSLR (Digital Single Lens Reflex) cameras such as the Canon 5D MarkIV.

Wide-FOV imaging is achieved by stitching multiple images that are recorded from the same center of projection [11]. Stitched images produce a better spatial resolution, but the parallax between the views produce artifacts on the resulting image. This issue is addressed by the LF panorama stitching [12]. Unfortunately, both strategies require a sequential capture, thus dedicated to static scenes. Changing the main-lens for a wider FOV lens is another solution, but these lenses are often bulky and require larger stack of lenses to produce sharp images. Alternatively, monocentric lenses [13], [14] have become increasingly popular for gigapixel imaging [15]. With these lenses, the light is collected on a spherical surface either with a curved sensor or a fiber coupling interface to a flat sensor. This approach has been pushed further using a plenoptic camera [16]. Finally, combining a prism array with common cameras has been proposed to double [17] or quadruple [18] the FOV of the main-lens. [19], prisms and mirrors are combined for stereo capture out of a single lens camera.

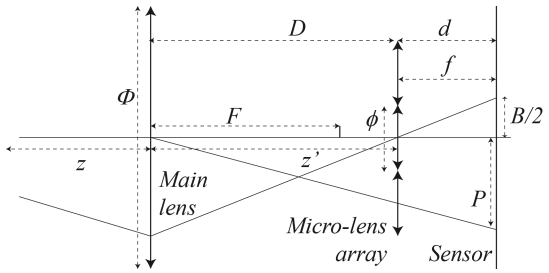

Fig. 1: Schematic view of a type-1 plenoptic camera.

Our contributions In this paper we analyze the advantages and constraints of plenoptic sensors. In particular, we focus on the so-called quad-pixel sensor where a micro-lens covers 2×2 pixels. In our study, we describe the relationship between the SAI's and the corresponding portions of the main-lens pupil through which light rays have travelled.

Besides, we propose an optical design for a single lens camera that doubles the FOV of the lens combining a plenoptic sensor and a pyramidal lens made of four prisms. The main idea is that the prisms deviate the photons entering the main-lens creating four distinct views that can be demultiplexed into the SAI's thanks to the plenoptic sensor. Then, with a single snapshot, the stitching of the SAI's increases the FOV up to a factor of two in each direction without changing the main-lens focal length, which is an unprecedented capability. Our experiments include synthetic image simulations and real images captured with two different prototypes we have constructed.

ISBN 978-90-827970-1-5

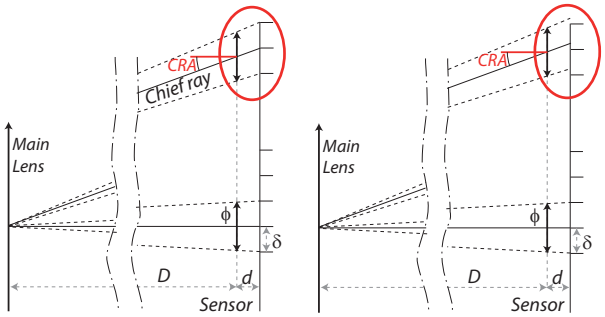

Fig. 2: Type-1 plenoptic camera with $N = 2$. Left: symmetric sampling of the micro-images when $\phi = 2\delta/e$. Right: asymmetric sampling of the micro-images when $\phi = 2\delta$ (considering $e = 1$). The Chief Ray Angle (CRA), the angle between one ray and the sensor is illustrated. The asymmetric sampling is said CRA corrected.

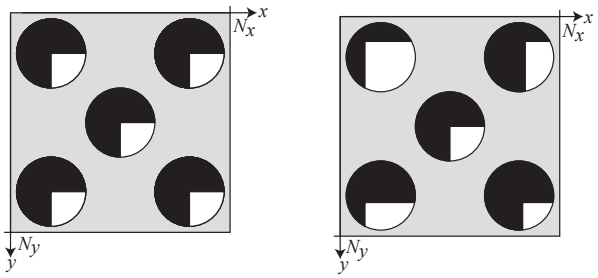

Fig. 3: Left: ideal portion of the exit pupil being visible by the SAI $S_{0,0}$ when $P = 2\delta$. This portion is constant independently of the sensor coordinate (x, y). Right: portion of the exit pupil visible by $\widehat{S}_{0,0}$ for a camera with $\phi = 2\delta$. The visible portion is asymmetric and depends on the position of the micro-image on the sensor as well as e.

II. From plenoptic cameras to plenoptic sensor

In this paper we focus on type-1 plenoptic sensors for its capacity to sample the main-lens exit pupil. Indeed, type-1 plenoptic cameras [1] are characterized by the fact that the distance d between the MLA and the sensor is equal to the micro-lenses focal length f (as illustrated in Fig. 1). So, the micro-lenses are imaging the main-lens exit pupil which is equal to the lens aperture in a thin lens model. The image on the pixels underneath the micro-lens is called micro-image.

Captured micro-images with $N \times N$ pixels, $N \in \mathbb{N}$, correspond to sampling the main-lens exit pupil with a $N \times N$ grid. For instance, if $N = 2$ (so called quad-pixel), each pixel of the 2×2 micro-image integrates the light rays passing through one of the four quarter-discs of the aperture stop. By contrast, in type-2 or focused plenoptic cameras ($d \neq f$) micro-lenses focus at a plane that does not match with the main-lens exit pupil [20].

A. Pupil sampling with the micro-images

The pitch of the micro-lenses ϕ is equal to $\phi = N\delta/e$, where $e = 1+d/D$ according to the intercept theorem. Ideally the distance P between two micro-images should be equal to an integer number of pixels. This is, $P = N\delta$, with δ being the pixel size. Thus the micro-lenses should have a pitch which is slightly smaller than N pixels and is function of the main-lens distance D. Fig. 2 illustrates the micro-images position with respect to the pixel array at the center of the sensor and at the border.

Sensor manufacturer are able to produce MLA having a pitch slightly smaller than the pixel size δ [21], [22]. This fact emphasizes how ready are manufacturers to produce quad-pixels plenoptic sensor such that the chief ray (the ray at the center of the micro-image) hit the middle of the 2×2 pixels (as illustrated in Fig. 2-left).

B. Study of SAI's on the Plenoptic Sensor

Collecting the SAI's is simple thanks to the integer size $N \times N$ of the micro-images. Let $L(x, y)$ be the image captured by the sensor with $(x, y) \in [0, N_x[\times[0, N_y[$. Then, the SAI's $S_{i,j},\ [i, j] \in [0, N[^2$ are obtained by simple demultiplexing:

$$S_{i,j}(k, l) = L\left(\left\{\left\lfloor \frac{x}{N} \right\rfloor + i\right\} \bmod N,\ \left\{\left\lfloor \frac{y}{N} \right\rfloor + j\right\} \bmod N\right) \quad (1)$$

where $(k, l) = (\lfloor x/N \rfloor, \lfloor y/N \rfloor) \in [0, N_x/N] \times [0, N_y/N]$. If the micro-lens pitch ϕ is not exactly equal to $N\delta/e$, then P is not an integer number of pixels, and computing the SAI's with Eq. 1 is incorrect. Indeed, by definition SAI's require to collect pixels at a fixed distance from the micro-image centers. So, if $P \neq N\delta$, SAI computation requires interpolation to extract pixels at non-integer coordinates from the sensor image [5]. Such interpolation averages micro-image pixels, mixing the angular information encoded in the micro-images. To prevent it, Eq. 1 is nevertheless used to extract approximate SAI's that we note $\widehat{S}_{i,j}$.

It is interesting to point out that the micro-images sample the main-lens exit pupil with a constant partition when $P = N\delta$ regardless of the micro-image position on the sensor. On the contrary, when $P \neq N\delta$, the approximate SAI's do not sample the main-lens exit pupil homogeneously. Fig. 3 illustrates the portion of the pupil visible by the SAI $S_{(0,0)}$ of a quad-pixel $(N = 2)$ type-1 plenoptic sensor.

Until now, we have modelled the main-lens with a thin lens model. However, considering the real-lens is mandatory to understand how the main-lens exit pupil is sampled. The real-lens pupil, also named the aperture stop, is the physical stop delimiting the beam of photons entering the camera. The aperture stop is located where a diaphragm can reduce homogeneously the amount of light on the sensor. Most lenses designed for DSLR cameras have an aperture stop roughly located within the main-lens. On the contrary, for smartphones, the aperture stop is mostly located at the entrance of the main-lens [23]. In this paper, we consider main-lenses where the aperture stop is positioned at the first diopter on the opposite side of the sensor.

ISBN 978-90-827970-1-5 © EURASIP 2018

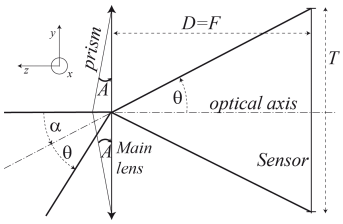

Fig. 4: Sensor and main-lens mounted with two prisms.

III. Doubling the FOV

Extending the FOV with a pyramid lens With a common camera, θ the half FOV of an image is given by the focal length F of the main-lens and the physical size T of the sensor: $\theta = \arctan \frac{T}{2F}$.

To extend the FOV, a pyramid lens (*i.e.*four prisms assembled together) is placed at the main-lens aperture stop. The FOV per portion of the pupil is rotated in different orientations. Each prism deviates the photons entering the main-lens by an angle α with respect to the x axis. α is chosen to be equal to the half FOV angle θ of the main-lens. With the two prisms of Fig. 4, the sensor records the superposition of two images, each one imaging a different part of the main-lens exit pupil. These two superposed images, combined together, double the FOV in the vertical direction of the camera. Similarly, using four prisms in front of the main-lens, each one covering a quarter of the main-lens aperture stop, doubles the FOV of the camera in vertical and horizontal orientations.

The angle α associated with the prism is function of its angle A and the refraction index n of its material. A good approximation gives $\alpha \approx (n-1)A$. Since α is set to be equal than θ, the prism angle A is easily computed knowing the refraction index of the prism material.

Extending the FOV with a plenoptic sensor Discriminating the two or four images that have been summed at the sensor plane is not easy. It requires to know which prism the photon has crossed. This is done with a plenoptic sensor with an ideal pupil sampling. Considering a quad-pixel sensor, the four SAI's are stitched to produce a single image that has a double FOV, as many pixels as the sensor and a single exposure time. Note that the equivalent f-number of the stitched image is divided by two, since SAI's collect only a quarter of the incoming photons.

IV. Image simulation

Simulated images are generated with PBRT [24] which has been extended to support an array of prisms and a MLA [25]). In particular, a ray is cast within a cone which is defined by an apex located on the sensor and a disk-shaped base which is defined by the exit pupil diameter of the main-lens and is located at the exit pupil position from the sensor. The ray is then refracted according to the thin lens model or Snell-Descartes law for the prism.

Synthetic images are generated with the ideal thin lens model (for both main- and micro-lenses). The plenoptic camera characteristics are defined in Table I. A test chart of colored letters and numbers is located at $z = 2m$ from the camera, a red disk indicates its center. A green cross located at $z = 0.5m$ is positioned on the main-lens optical axis. Four prisms forming a pyramid are positioned at the main-lens aperture stop. Each prism is defined by a material with a constant refraction index of $n = 1.74$ and an angle of $A = 16.7°$.

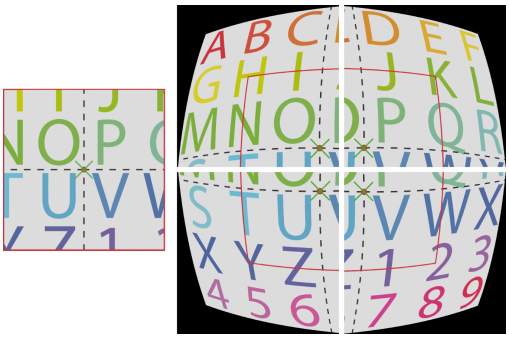

Fig. 5: Left: One of the four identical SAI's when there is no prism. Right: Different simulated SAI's obtained with a pyramid lens. The red dot on the left and red square on the right of the test chart indicate respectively the optical axis of the main-lens.

$F = 6.16mm$	$\Phi = 3.09mm$	$D = 6.18mm$
$f = 4.8\mu m$	$\phi = 2.3981\mu m$	$d = f$
$\delta = 1.2\mu m$	$N_x N_y = 3000^2$	$T = 3.6mm$

TABLE I: Ideal plenoptic camera characteristics.

Fig. 5 illustrates the SAI's extracted from the synthetic simulation. Without prisms the four SAI's are identical whereas with the four prisms, each SAI observes a deviated FOV. The observed distortions are due to the prism. Cancelling the constant geometrical distortion enables to stitch trivially the four SAI's into a single image having almost the size of the sensor. The FOV of the main-lens was $32°$, and with the prisms becomes $64°$.

The prisms being located by design at the entrance pupil of the main-lens, the 4 rotated SAI's have the same perspective and are not affected by parallax error. This is confirmed by the green crosses which match the red disks. One deduces that no parallax error are visible. More precisely, parallax error occurs for out-of-focus objects since the blur function associated to a SAI is a quarter disk which by convolution produces a tiny shift function of the defocus.

V. Extended FOV with a type-2 camera

We ideally would experiment with a type-1 camera, but the Raytrix camera is the only available plenoptic camera which enables to change the main-lens. Indeed, a main-lens with an aperture stop located at its entrance is required for our experiment. In particular, the experiment we have set up allows to double horizontally the FOV of a main-lens mounted with the Raytrix R5 camera.

ISBN 978-90-827970-1-5 © EURASIP 2018

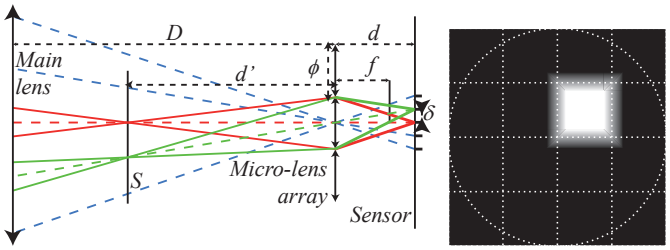

Fig. 6: Type-2 plenoptic camera with $P = 4\delta = \phi e$ Left: Scheme in 1D. Red and green lines indicate the ray beams which exit at the border of the pixel of size δ, converging on two points at plane S and diverging on the main-lens. The colored dashed lines delimit the four projected pixels of one micro-lens into the main-lens pupil. Right: Pupil sampling in 2D with the portion of the pupil seen by one pixel in white. Fading regions represent visibility overlapping.

A. Type-2 pupil sampling

As mentioned before, micro-lenses in type-2 cameras do not focus at the main-lens exit pupil but at a plane S distant by d' from the MLA. Thus, the main-lens exit pupil is not sampled with a disjoint partition. Instead, corresponding pixel visibility areas overlap (see Fig.6). The overlap thickness between two juxtaposed portions is function of the ratio f/d and the pupil diameter Φ.

B. Converting a type-2 into a dual-pixel camera

Dual-pixel refers to a plenoptic sensor having 2 rectangular pixels bellow each micro-lens. It enables to capture 2 SAI's. Our experiment converts the Raytrix camera into a dual-pixel camera. Our prototype has only one prism to deviate half of the photons entering the main-lens. The main-lens needs to be sufficiently thin, so the prism can be set as close as possible to it. We assume the prism to be placed at the main-lens aperture stop.

The Raytrix R5 has many pixels per micro-lens ($P = 20.20\,\delta$). To convert it into a dual-pixel camera, stereo refocused images are computed splitting the left and right portions of the micro-images. The two refocused images are comparable to the SAI's extracted from a dual-pixel sensor. We have used the pipeline in [6] to compute the two refocused images from the Raytrix R5. We summarize the main steps bellow:

Micro-lens image calibration The MLA is an hexagonal lattice fully characterized by a radius, a rotation angle (with respect to the pixel matrix) and the offset between the first micro-image center and the origin of the sensor. These values are all computed using the Fourier transform of a white image, this is a shot of a flat white screen homogeneously illuminated. The calibration associates a pixel coordinate (x, y) with a micro-lens coordinate (i, j).

Micro-lens vignetting correction The white image is normalized by its average maximum and inverted to define a flux scaled correction per pixel that fixes the vignetting of the micro-images.

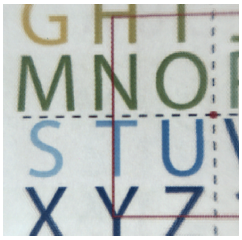

(a) Full refocus no prism.

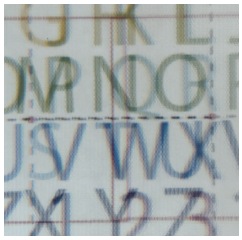

(b) Full refocus with prism.

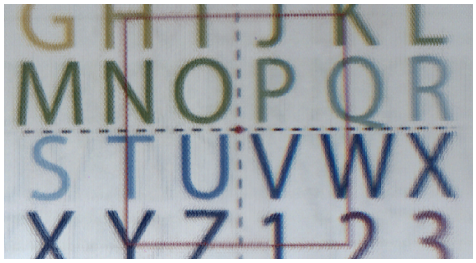

(c) SAI stitching.

Fig. 7: Raytrix refocus and stitching.

Stereo image refocusing Image refocusing with a type-2 camera is defined with Eq. 2:

$$\begin{bmatrix} X \\ Y \end{bmatrix} = s\left(g\left(\begin{bmatrix} x \\ y \end{bmatrix} - \begin{bmatrix} x_{i,j} \\ y_{i,j} \end{bmatrix}\right) + \begin{bmatrix} x_{i,j} \\ y_{i,j} \end{bmatrix}\right) \tag{2}$$

Where (X, Y) is the projection on the refocused image of the sensor pixel (x, y) which belongs to micro-image (i, j). Micro-image (i, j) is centered at pixel coordinate $(x_{i,j}, y_{i,j})$. g controls the refocalization distance, and s the relative size of the refocused image versus the input LF image. A weight-map is maintained to count the projected pixels. The refocused image is normalized with the weight-map after all pixels are projected.

The left and right refocused images are computed with Eq. 2 and the following conditions respectively $(x - x_{i,j}) < -m/2$ and $(x - x_{i,j}) > m/2$. Where m is the thickness in pixels of the vertical masks located at the middle of the micro-images to cancel sub-aperture cross-talk.

The refocalization parameters are set to $s = 0.2$ (refocused images are 5 times smaller than the input image) and $g = 4$. The test chart is positioned such that the images appear as sharp as possible. Experimentally m is set to 2 to cancel the cross-talk.

Extended image stitching The prism produces small distortions and the two refocused images are stitched using a simple horizontal translation to match their two common portions. This process can further be totally automatized.

Common refocused images considering all the pixels below the micro-lens are shown at the top of Fig. 7 with and without the prism covering half of the main-lens pupil. The stitched SAI's are visible in Fig. 7c.

VI. Application with a dual-pixel camera

The primary goal of dual-pixel sensor is to perform live auto-focus for video shooting. Recently, with the 5D MarkIV,

ISBN 978-90-827970-1-5 © EURASIP 2018

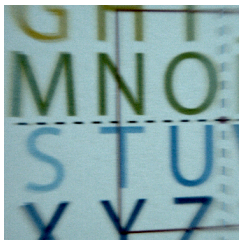

(a) Full refocus no prism.

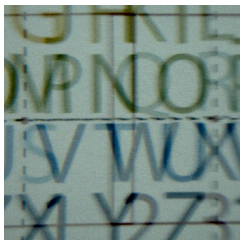

(b) Full refocus with prism.

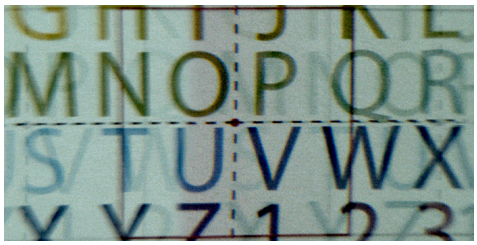

(c) SAI stitching.

Fig. 8: Canon 5D MarkIV refocus and stitching.

Canon gives access to the raw dual-pixel.

The raw images are processed with the following steps: 1/ The raw files are read with [26], 2/ The SAI are bias-corrected thanks to over-scan areas which are then cropped to keep the responsive pixels, 3/ A white screen is observed with the same lens used with the Raytrix camera, the two SAI's are median filtered, normalized by their maxima, and inverted to define a flux-scale correction which is applied to all captured images. Due to the poor quality of the main-lens, only a central portion of $2000^2 pix$ is used.

The images captured with and without the prism are shown at the top of Fig. 8 The two SAI's obtained with the prism are stitched to form an extended FOV image (see Fig. 8c).

Note that on the stitched image, a ghost image is clearly visible, despite the use of a central large mask, masking most of the aperture stop. Actually, we have discovered that the dual-pixel sensor designed by Canon does not produce a sharp sampling of the main-lens pupil.

VII. Discussion and Conclusion

In the future, ideal quad-pixel sensors could be used in two distinct modes: 1/ the four SAI's are used with typical plenoptic algorithms (e.g. refocus[9], depth-estimation [27], partial lens aberration correction [28]) without previous micro-lens center estimation which is a cumbersome task, or 2/ as proposed in this paper, combined with a pyramid lens and stitching the different SAI's to double the FOV as well as the spatial resolution. The pyramid lens would be used as a conversion lens. These two options are especially suitable for smartphones which use a fixed focal lens, and presumably soon a quad-pixel sensor (dual-pixels already integrated).

To complete this study, several technical aspects are to be pointed out: 1/ The SAI's collect photons passing by a quarter disk in the case of a quad-pixel sensor. Thus, we effectively trade the amount of light dedicated to image a scene point against an increase in FOV. 2/ The main-lens has to be designed with an aperture stop located at its entrance and 3/ prisms produce strong chromatic aberrations that degrade the image quality of SAI's, achromatic prisms could be used to decrease chromatic aberrations.

References

[1] R. Ng, "Digital light field photography," Ph.D. dissertation, Stanford, CA, USA, 2006.

[2] "https://www.lytro.com."

[3] A. Lumsdaine and T. Georgiev, "The focused plenoptic camera," in *ICCP*, 2009, pp. 1–8.

[4] "http://www.raytrix.de."

[5] D. G. Dansereau, O. Pizarro, and S. B. Williams, "Decoding, calibration and rectification for lenselet-based plenoptic cameras," in *CVPR*, 2013, pp. 1027–1034.

[6] M. Hog, N. Sabater, B. Vandame, and V. Drazic, "An image rendering pipeline for focused plenoptic cameras," *IEEE Trans. on Computational Imaging*, vol. 3, no. 4, pp. 811–821, 2017.

[7] D. Cho, M. Lee, S. Kim, and Y.-W. Tai, "Modeling the calibration pipeline of the lytro camera for high quality light-field image reconstruction," in *ICCV*, 2013, pp. 3280–3287.

[8] N. Sabater, M. Seifi, V. Drazic, G. Sandri, and P. Perez, "Accurate disparity estimation for plenoptic images," in *ECCV Workshop*, 2014.

[9] J. Fiss, B. Curless, and R. Szeliski, "Refocusing plenoptic images using depth-adaptive splatting," in *ICCP*, 2014, pp. 1–9.

[10] S. Choi, K. Lee, J. Yun, S. Choi, S. Lee *et al.*, "An all pixel pdaf cmos image sensor with $0.64\mu m$x$1.28\mu m$ photodiode separated by self-aligned in-pixel deep trench isolation for high af performance," in *Symp. on VLSI Technology*, 2017, pp. T104–T105.

[11] R. Szeliski and H.-Y. Shum, "Creating full view panoramic image mosaics and environment maps," in *SIGGRAPH*, 1997, pp. 251–258.

[12] P. P. M. V. Zhou Xue, Loic Baboulaz, "Light field panorama by a plenoptic camera," in *SPIE*, vol. 9020, 2014.

[13] I. Stamenov, I. P. Agurok, and J. E. Ford, "Optimization of two-glass monocentric lenses for compact panoramic imagers: general aberration analysis and specific designs," *Appl. Opt.*, vol. 51, no. 31, pp. 7648–7661, 2012.

[14] I. Stamenov, A. Arianpour, S. J. Olivas, I. P. Agurok, A. R. Johnson *et al.*, "Panoramic monocentric imaging using fiber-coupled focal planes," *Opt. Express*, vol. 22, no. 26, pp. 31 708–31 721, 2014.

[15] O. S. Cossairt, D. Miau, and S. K. Nayar, "Gigapixel computational imaging," in *ICCP*, 2011, pp. 1–8.

[16] D. G. Dansereau, G. Schuster, J. Ford, and G. Wetzstein, "A wide-field-of-view monocentric light field camera," in *CVPR*, 2017.

[17] C.-Y. Chen, T.-T. Yang, and W. S. Sun, "Optics system design applying a micro-prism array of a single lens stereo image pair," *Opt. Express*, vol. 16, no. 20, pp. 15 495–15 505, 2008.

[18] W.-S. Sun, C.-L. Tien, C.-Y. Chen, and D.-C. Chen, "Single-lens camera based on a pyramid prism array to capture four images," *Optical Review*, vol. 20, no. 2, pp. 145–152, 2013.

[19] G. Somanath, M. V. Rohith, and C. Kambhamettu, *Single Camera Stereo System Using Prism and Mirrors*, 2010, pp. 170–181.

[20] T. Georgiev and A. Lumsdaine, "Focused plenoptic camera and rendering," *Journal of Electronic Imaging*, vol. 19, no. 2, p. 021106, 2010.

[21] Y. Sekine, "Solid state image sensor, method of manufacturing solid state image sensor, and image capturing system," 2016, uS Patent App. 15/010,340.

[22] A. E. G. Peter Bert Catrysse, Xinqiao Liu, "Qe reduction due to pixel vignetting in cmos image sensors," vol. 3965, 2000, pp. 3965–11.

[23] R. Mercado, "Small form factor telephoto camera," 2015, uS Patent App. 14/069,027.

[24] M. Pharr and G. Humphreys, *Physically Based Rendering, Second Edition: From Theory To Implementation*, 2nd ed. San Francisco, CA, USA: Morgan Kaufmann Publishers Inc., 2010.

[25] C. Kolb, D. Mitchell, and P. Hanrahan, "A realistic camera model for computer graphics," in *SIGGRAPH*. ACM, 1995, pp. 317–324.

[26] "Libraw library," http://www.libraw.org/.

[27] M. W. Tao, P. P. Srinivasan, J. Malik, S. Rusinkiewicz, and R. Ramamoorthi, "Depth from shading, defocus, and correspondence using light-field angular coherence," in *CVPR*, 2015, pp. 1940–1948.

[28] P. Hanrahan and R. Ng, "Digital correction of lens aberrations in light field photography," in *Int. Optical Design*, 2006.

ISBN 978-90-827970-1-5 © EURASIP 2018